

Augmenting optimization-based molecular design with graph neural networks

Shiqiang Zhang^a, Juan S. Campos^a, Christian Feldmann^b, Frederik Sandfort^b, Miriam Mathea^b, Ruth Misener^a

^aImperial College London, London, UK

^bBASF SE, Ludwigshafen, Germany

Abstract

Computer-aided molecular design (CAMD) studies quantitative structure-property relationships and discovers desired molecules using optimization algorithms. With the emergence of machine learning models, CAMD score functions may be replaced by various surrogates to automatically learn the structure-property relationships. Due to their outstanding performance on graph domains, graph neural networks (GNNs) have recently appeared frequently in CAMD. But using GNNs introduces new optimization challenges. This paper formulates GNNs using mixed-integer programming and then integrates this GNN formulation into the optimization and machine learning toolkit OMLT. To characterize and formulate molecules, we inherit the well-established mixed-integer optimization formulation for CAMD and propose symmetry-breaking constraints to remove symmetric solutions caused by graph isomorphism. In two case studies, we investigate fragment-based odorant molecular design with more practical requirements to test the compatibility and performance of our approaches.

Keywords: Optimization formulations, Molecular design, Graph neural networks, Inverse problem, Software tools

1. Introduction

Computer-aided molecular design (CAMD) uses modeling and optimization algorithms to discover and develop new molecules with desired properties (Gani, 2004; Ng et al., 2014; Austin et al., 2016; Chong et al., 2022; Gani et al., 2022; Mann et al., 2023). Recent CAMD advances use the rapid devel-

opment of machine learning to create surrogate models which learn structure-property relationships and can then score and/or generate molecules (Elton et al., 2019; Alshehri et al., 2020, 2021; Faez et al., 2021; Gao et al., 2022; Hatamleh et al., 2022; Tiew et al., 2023). CAMD also heavily relies on numerical optimization algorithms to find reasonable and promising candidates in a specific design space: the resulting optimization problems are typically non-convex and nonlinear (Camarda and Maranas, 1999; Ng et al., 2014; Zhang et al., 2015).

Due to the natural graph representation of molecules, graph neural networks (GNNs) are attractive in CAMD (Xia et al., 2019; Yang et al., 2019; Xiong et al., 2021; Rittig et al., 2022). GNNs can predict molecular properties given the graph structure of molecules (Gilmer et al., 2017; Xu et al., 2017; Shindo and Matsumoto, 2019; Wang et al., 2019; Schweidtmann et al., 2020; Withnall et al., 2020). Molecular design in these GNN-based approaches requires optimizing over graph domains. Most works use optimization algorithms such as genetic algorithms and Bayesian optimization that *evaluate* GNNs rather than directly handling the inverse problems defined on GNNs (Jin et al., 2018, 2020; Rittig et al., 2022). In these works, GNNs are typically used as forward functions during the optimization process. One exception is the work of McDonald et al. (2023), who first encoded both the graph structures of inputs and the inner structures of GNNs into a specific CAMD problem using mixed-integer programming.

Mixed-integer programming (MIP) can directly formulate molecules with optimization constraints. The basic idea is representing a molecule as a graph, creating variables for each atom (or group of atoms), and using constraints to preserve graph structure and satisfy chemical requirements. Such representations are well-established in the CAMD literature (Odele and Macchietto, 1993; Churi and Achenie, 1996; Camarda and Maranas, 1999; Sinha et al., 1999; Sahinidis et al., 2003; Zhang et al., 2015; Liu et al., 2019; Cheun et al., 2023). A score function with closed form is usually given as the optimization target. In addition to building the score function with knowledge from experts or statistics, we advocate using machine learning models, including GNNs, as score functions. But involving machine learning models brings new challenges to optimization: our work seeks to make it tractable to optimize over these models.

Mathematical optimization over trained machine learning models is an area of increasing interest. In this paradigm, a trained machine learning model is translated into an optimization formulation, thereby enabling decision-

making problems over model predictions. For continuous, differentiable models, these problems can be solved via gradient-based methods (Szegedy et al., 2014; Bunel et al., 2020b; Wu et al., 2020; Horvath et al., 2021). MIP has also been proposed, mainly to support non-smooth models such as ReLU neural networks (Fischetti and Jo, 2018; Anderson et al., 2020; Tsay et al., 2021), their ensembles (Wang et al., 2023), and tree ensembles (Mišić, 2020; Mistry et al., 2021; Thebelt et al., 2021). Optimization over trained ReLU neural networks has been especially prominent (Huchette et al., 2023), finding applications such as verification (Bunel et al., 2018; Tjeng et al., 2019; Botoeva et al., 2020; Bunel et al., 2020a), reinforcement learning (Say et al., 2017; Delarue et al., 2020; Ryu et al., 2020), compression (Serra et al., 2021), and black-box optimization (Papalexopoulos et al., 2022).

Motivated by the intersection of MIP, GNNs, and CAMD, our conference paper (Zhang et al., 2023) optimizes over trained GNNs with a molecular design application and combines mixed-integer formulations of GNNs and CAMD. By breaking symmetry caused by graph isomorphism, we reduced the redundancy in the search space and sped up the solving process. This paper extends this conference paper. Section 2 and Section 4 primarily derive from Zhang et al. (2023). The new contributions of this paper include:

- Improving the mixed-integer formulation of GNNs with tighter constraints in Section 2.3.
- Implementing the GNN encoding into the optimization and machine learning toolkit OMLT (Ceccon et al., 2022).
- Extending the mixed-integer formulation of CAMD from atom-based to fragment-based design in Section 5, this change admits larger molecules with aromaticity.
- Investigating two case studies in Section 5.1 and Section 5.2. We incorporate several practical requirements into our formulations to design more realistic molecules.

Paper structure Section 2 introduces optimization over trained GNNs. Section 3 discusses the implementation of GNNs in OMLT. Section 4 presents the mixed-integer formulation for CAMD and symmetry-breaking constraints. Section 5 shows two case studies with specific requirements. Section 6 provides numerical results. Section 7 concludes and discusses future work.

2. Optimization over trained graph neural networks

2.1. Definition of graph neural networks

This work considers a GNN with L layers:

$$GNN : \underbrace{\mathbb{R}^{d_0} \otimes \dots \otimes \mathbb{R}^{d_0}}_{|V| \text{ times}} \rightarrow \underbrace{\mathbb{R}^{d_L} \otimes \dots \otimes \mathbb{R}^{d_L}}_{|V| \text{ times}},$$

where V is the set of nodes of the input graph. Let $\mathbf{x}_v^{(0)} \in \mathbb{R}^{d_0}$ be the input features for node v . Then, the l -th layer ($l = 1, 2, \dots, L$) is defined by:

$$\mathbf{x}_v^{(l)} = \sigma \left(\sum_{u \in \mathcal{N}(v) \cup \{v\}} \mathbf{w}_{u \rightarrow v}^{(l)} \mathbf{x}_u^{(l-1)} + \mathbf{b}_v^{(l)} \right), \quad \forall v \in V, \quad (l^{\text{th}} \text{ layer})$$

where $\mathcal{N}(v)$ is the set of all neighbors of v and σ is any activation function.

With linear aggregate functions such as sum and mean, many classic GNN architectures can be rewritten in form (l^{th} layer), e.g., Spectral Network (Bruna et al., 2014), Neural FPs (Duvenaud et al., 2015), DCNN (Atwood and Towsley, 2016), ChebNet (Defferrard et al., 2016), PATCHY-SAN (Niepert et al., 2016), MPNN (Gilmer et al., 2017), GraphSAGE (Hamilton et al., 2017), and GCN (Kipf and Welling, 2017).

2.2. Problem definition

Given a trained GNN in form (l^{th} layer), we consider optimization problems defined as:

$$\begin{aligned} \min_{(\mathbf{x}_v^{(0)}, \dots, \mathbf{x}_v^{(L)}, A)} \quad & \text{obj}(\mathbf{x}_v^{(0)}, \dots, \mathbf{x}_v^{(L)}, A) & (\text{OPT}) \\ \text{s.t.} \quad & f_i(\mathbf{x}_v^{(0)}, \dots, \mathbf{x}_v^{(L)}, A) \leq 0, i \in \mathcal{I}, \\ & g_j(\mathbf{x}_v^{(0)}, \dots, \mathbf{x}_v^{(L)}, A) = 0, j \in \mathcal{J}, \\ & (l^{\text{th}} \text{ layer}), 1 \leq l \leq L, \end{aligned}$$

where A is the adjacency matrix of input graph, f_i, g_j are problem-specific constraints and \mathcal{I}, \mathcal{J} are index sets.

2.3. Mixed-integer optimization formulations for graph neural networks

If the graph structure for inputs is given and fixed, then a GNN layer in form (l^{th} layer) is equivalent to a dense, i.e., fully connected, layer, whose MIP formulations are established (Anderson et al., 2020; Tsay et al., 2021). But if the graph structure is non-fixed, the elements in adjacency matrix A are also decision variables.

Assuming that the weights and biases are constant, Zhang et al. (2023) developed both a bilinear and a big-M formulation. The bilinear formulation results in a mixed-integer quadratically constrained optimization problem, which can be handled by state-of-the-art solvers. The Zhang et al. (2023) big-M formulation generalizes McDonald et al. (2023) from GraphSAGE (Hamilton et al., 2017) to all GNN architectures satisfying (l^{th} layer). The Zhang et al. (2023) numerical results show that the big-M formulation outperforms the bilinear one in both (i) the time when the optimal solution was found and (ii) the time spend proving that this solution is optimal, so this paper only introduces the big-M formulation.

The big-M formulation adds auxiliary variables $\mathbf{z}_{u \rightarrow v}^{(l-1)}$ to represent the contribution from node u to node v in the l -th layer:

$$\mathbf{x}_v^{(l)} = \sigma \left(\sum_{u \in V} \mathbf{w}_{u \rightarrow v}^{(l)} \mathbf{z}_{u \rightarrow v}^{(l-1)} + \mathbf{b}_v^{(l)} \right), \quad \forall v \in V, \quad (\text{big-M})$$

where $\mathbf{z}_{u \rightarrow v}^{(l-1)} = A_{u,v} \mathbf{x}_u^{(l-1)}$ is constrained using big-M:

$$\begin{aligned} \mathbf{x}_u^{(l-1)} - \mathbf{U}_u^{(l-1)}(1 - A_{u,v}) &\leq \mathbf{z}_{u \rightarrow v}^{(l-1)} \leq \mathbf{x}_u^{(l-1)} - \mathbf{L}_u^{(l-1)}(1 - A_{u,v}), \\ \mathbf{L}_u^{(l-1)} A_{u,v} &\leq \mathbf{z}_{u \rightarrow v}^{(l-1)} \leq \mathbf{U}_u^{(l-1)} A_{u,v}, \end{aligned}$$

where $\mathbf{L}_u^{(l-1)} \leq \mathbf{x}_u^{(l-1)} \leq \mathbf{U}_u^{(l-1)}$, $A_{u,v} \in \{0, 1\}$. Given the bounds of input features $\{\mathbf{x}_v^{(0)}\}_{v \in V}$, all bounds of $\{\mathbf{x}_v^{(l)}\}_{v \in V, 1 \leq l \leq L}$ can be derived using interval arithmetic. Note that these big-M constraints provide tighter bounds for $\mathbf{z}_{u \rightarrow v}^{(l-1)}$ than the original Zhang et al. (2023) formulation.

3. Encoding graph neural networks into OMLT

OMLT (Ceccon et al., 2022) is an open-source software package that encodes trained machine learning models into the algebraic modeling language Pyomo (Bynum et al., 2021). Taking a trained dense neural network as

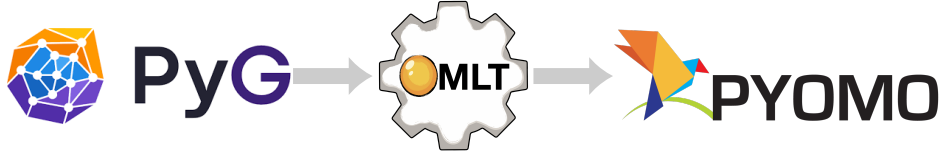


Figure 1: With the contributions in this paper, OMLT now transforms a PyG GNN sequential model into a Pyomo block.

an example, by defining variables for all neurons and adding constraints to represent links between layers, OMLT automatically transforms the neural network into a Pyomo block suitable for optimization. Currently, OMLT supports dense neural networks (Anderson et al., 2020; Tsay et al., 2021), convolutional neural networks (Albawi et al., 2017), gradient-boosted trees (Thebelt et al., 2021), and linear model decision trees (Ammari et al., 2023).

To enable GNNs in OMLT, we create a **GNNLayer** class defined by (l^{th} layer) and encode this class using the Section 2.3 big-M formulation. As shown in Figure 1, our extension to OMLT now supports GNNs through a Pytorch Geometric PyG (Fey and Lenssen, 2019) interface. Note that OMLT requires a sequential GNN model in PyG as a standard format.

In this section, we first describe the **GNNLayer** class and provide some examples to show how to transform various GNN-relevant operations to OMLT in Section 3.1. Section 3.2 shows details about encoding **GNNLayer**. Section 3.3 lists all currently supported operations in our extension to OMLT.

3.1. *GNNLayer* class in OMLT

The OMLT **GNNLayer** class requires the following information:

- N : number of nodes.
- Input/Output size: number of input/output features for all nodes. Note that the input/output size should be equal to N multiplied by the number of input/output features for each node.
- Weight matrix \mathbf{W} : consists of all weights $\mathbf{w}_{u \rightarrow v}$, $\forall u, v \in [N]$.
- Biases \mathbf{B} : consists of all biases \mathbf{b}_v , $\forall v \in [N]$.

where $[N] := \{0, 1, \dots, N - 1\}$.

As long as a GNN layer satisfies definition (l^{th} layer), it could be defined in the **GNNLayer** class and encoded using (big-M). The extra effort is that

users need to properly transform their GNN layers to OMLT. We provide several examples to illustrate how to define a GNN layer inside OMLT.

Remark: This section only considers a single layer and drops the indexes of layers. To differentiate the input and output features, we use \mathbf{y}_v as the output features of node v .

Example 1 [Linear] Consider a linear layer:

$$\mathbf{y}_v = \mathbf{w}^T \mathbf{x}_v + \mathbf{b}, \forall v \in [N].$$

This is different from a common dense layer since it works on features of each node separately. Our new extension to OMLT transforms this layer into a dense layer with parameters:

$$\mathbf{W} = \begin{pmatrix} \mathbf{w} & & & \\ & \mathbf{w} & & \\ & & \ddots & \\ & & & \mathbf{w} \end{pmatrix}, \mathbf{B} = \begin{pmatrix} \mathbf{b} \\ \mathbf{b} \\ \vdots \\ \mathbf{b} \end{pmatrix}.$$

Example 2 [GCNConv with fixed graph] Given a GCNConv layer:

$$\mathbf{y}_v = \mathbf{w}^T \sum_{u \in \mathcal{N}(v) \cup \{v\}} \frac{A_{u,v}}{\sqrt{\hat{d}_u \hat{d}_v}} \mathbf{x}_u + \mathbf{b}, \forall v \in [N],$$

where $\hat{d}_v = 1 + \sum_{u \in \mathcal{N}(v)} A_{u,v}$. Our new extension to OMLT defines a GNN layer in OMLT with parameters:

$$\mathbf{W} = \begin{pmatrix} \frac{A_{0,0}}{\sqrt{\hat{d}_0 \hat{d}_0}} \mathbf{w} & \frac{A_{0,1}}{\sqrt{\hat{d}_0 \hat{d}_1}} \mathbf{w} & \cdots & \frac{A_{0,N-1}}{\sqrt{\hat{d}_0 \hat{d}_{N-1}}} \mathbf{w} \\ \frac{A_{1,0}}{\sqrt{\hat{d}_1 \hat{d}_0}} \mathbf{w} & \frac{A_{1,1}}{\sqrt{\hat{d}_1 \hat{d}_1}} \mathbf{w} & \cdots & \frac{A_{1,N-1}}{\sqrt{\hat{d}_1 \hat{d}_{N-1}}} \mathbf{w} \\ \vdots & \vdots & \ddots & \vdots \\ \frac{A_{N-1,0}}{\sqrt{\hat{d}_{N-1} \hat{d}_0}} \mathbf{w} & \frac{A_{N-1,1}}{\sqrt{\hat{d}_{N-1} \hat{d}_1}} \mathbf{w} & \cdots & \frac{A_{N-1,N-1}}{\sqrt{\hat{d}_{N-1} \hat{d}_{N-1}}} \mathbf{w} \end{pmatrix}, \mathbf{B} = \begin{pmatrix} \mathbf{b} \\ \mathbf{b} \\ \vdots \\ \mathbf{b} \end{pmatrix}.$$

Since A is given and fixed, all coefficients $\frac{A_{u,v}}{\sqrt{\hat{d}_u \hat{d}_v}}$ are constant. \mathbf{w}, \mathbf{b} are also constant for a trained GNN. Therefore, \mathbf{W}, \mathbf{B} are constant. However, when A is not fixed, a GCNConv layer results in the nonlinear formulation:

$$\mathbf{y}_v = \sum_{u \in [N]} \frac{A_{u,v}}{\sqrt{(1 + \sum_{w \in \mathcal{N}(u)} A_{w,u})(1 + \sum_{w \in \mathcal{N}(v)} A_{w,v})}} \mathbf{w}^T \mathbf{x}_u + \mathbf{b}, \forall v \in [N].$$

problem. All problem-specific variables and constraints can also be included into the block to represent practical requirements.

With the new **GNNLayer** class in OMLT, the last step is encoding the (big-M) formulation in Section 2.3 and associating it with **GNNLayer** by:

1. Defining binary variables $A_{u,v}, u, v \in [N]$ for all elements in the adjacency matrix A . Note: these variables are shared by all GNN layers.
2. defining variables for all features $\mathbf{x}_v^{(l)}, v \in [N], 0 \leq l \leq L$.
3. Defining auxiliary variables $\mathbf{z}_{u \rightarrow v}^{(l-1)}, u, v \in [N], 1 \leq l \leq L$.
4. Defining bounds $\left[\mathbf{L}_{u \rightarrow v}^{(l-1)}, \mathbf{U}_{u \rightarrow v}^{(l-1)} \right]$ for $\mathbf{z}_{u \rightarrow v}^{(l-1)}, u, v \in [N], 1 \leq l \leq L$ as:

$$\begin{cases} [\mathbf{0}, \mathbf{0}], & A_{u,v} \text{ is fixed to } 0 \\ \left[\mathbf{L}_u^{(l-1)}, \mathbf{U}_u^{(l-1)} \right], & A_{u,v} \text{ is fixed to } 1 \\ \left[\min(\mathbf{0}, \mathbf{L}_u^{(l-1)}), \max(\mathbf{0}, \mathbf{U}_u^{(l-1)}) \right], & A_{u,v} \text{ is not fixed} \end{cases}$$

where $\left[\mathbf{L}_u^{(l-1)}, \mathbf{U}_u^{(l-1)} \right]$ are bounds of $\mathbf{x}_u^{(l-1)}$.

5. Adding constraints to represent (big-M).

After formulating the **GNNLayer** class, we finish the implementation of GNNs in OMLT. For simplicity of notations, we only consider a GNN defined as (l^{th} layer). Benefiting from the layer-based architecture of OMLT, all layers that OMLT currently supports are compatible with the GNN encoding, as long as the outputs of the previous layer match the inputs of the next layer. For instance, OMLT can encode a GNN consisting of several GNN layers, a pooling layer, and several dense layers.

3.3. Supported PyG operations in OMLT

This section discusses our implementation of PyG operations in OMLT to facilitate GNN encoding. Table 1 summarizes all implemented operations with fixed or non-fixed graph structure. By assembling a GNN sequential model consisting of these operations, users may encode GNNs into OMLT without bothering with the complex transformations from Section 3.1.

As discussed in Section 2.3, when the input graph structure is not fixed, our extension of OMLT assumes constant weights and biases to formulate a GNN layer. The cost for this assumption is that **GCNConv** and **mean** aggregation are not supported in this case since both result in difficult mixed-integer nonlinear optimization problems, e.g., as shown in Example 2.

Table 1: Supported PyG operations in OMLT.

Type	Operations	Graph structure	
		fixed	non-fixed
Convolution	Linear	✓	✓
	GCNConv	✓	×
	SAGEConv	✓	✓
Aggregation	mean	✓	×
	sum	✓	✓
Pooling	global_mean_pooling	✓	✓
	global_add_pooling	✓	✓

In OMLT, activation functions are detached from layers. Therefore, all activation functions in OMLT are compatible with GNNs, including **ReLU**, **Sigmoid**, **LogSoftmax**, **Softplus**, and **Tanh**. Among these activations, ReLU can be represented by linear constraints using a big-M formulation (Anderson et al., 2020). Because of the binary variables $A_{u,v}$ representing the existence or not of an edge (see Section 2.3), any activation function formulated with nonlinear constraints will result in a mixed-integer nonlinear optimization problem. Thus, although OMLT will allow nonlinear activation functions for GNNs, practical algorithmic limitations may make nonlinear activations functions inadvisable in OMLT.

It is noteworthy that importing a GNN model from PyG interface is not the only way to encode GNNs in OMLT. One can transform their own GNNs into OMLT in a similar way to those examples in Section 3.1. As long as one can properly define their GNN operations into **GNNLayer** class, OMLT will formulate these layers using big-M automatically.

4. Mixed-integer optimization formulation for molecular design

MIP formulations are well-established in the CAMD literature. Our particular MIP formulation for CAMD starts with that of McDonald et al. (2023). Because our formulation also incorporates Sections 4.3.5 and 4.4, we are able to develop optimization approaches that find larger molecules (with 12 heavy atoms or fragments rather than 4).

4.1. Atom features

To design a molecule with at most N atoms, we define $N \times F$ binary variables $X_{v,f}, v \in [N], f \in [F]$ to represent F features for N atoms. Hydrogen atoms are not counted in since they can implicitly be considered as node features. Atom features include types of atom, number of neighbors, number of hydrogen atoms associated, and types of adjacent bonds. Table 2 summarizes relevant notations and provides their values for an example with four types of atoms $\{C, N, O, S\}$. Table 3 describes atom features explicitly.

4.2. Bond features

For bond features, we add three sets of binary variables $A_{u,v}, DB_{u,v}, TB_{u,v}$ to denote any bond, double bond, and triple bond between atom u and atom v , respectively:

- $A_{u,v}, u \neq v \in [N]$: if there is a bond between atom u and v .
- $A_{v,v}, v \in [N]$: if node v exists.
- $DB_{u,v}, u \neq v \in [N]$: if there is a double bond between atom u and v .
- $TB_{u,v}, u \neq v \in [N]$: if there is a triple bond between atom u and v .

Remark: $\{A_{v,v}\}_{v \in [N]}$ allow us to design molecules with at most N atoms. For comparison purposes in our experiments, however, we set $A_{v,v} = 1, \forall v \in [N]$ to design molecules with exactly N atoms.

4.3. Structural constraints

This section introduces constraints to handle structural feasibility, which is commonly considered in the literature (Odele and Macchietto, 1993; Churi and Achenie, 1996; Camarda and Maranas, 1999; Sinha et al., 1999; Sahinidis et al., 2003; Zhang et al., 2015).

4.3.1. Feasible adjacency matrix

Constraints (C1) represent the minimal requirement, i.e., there are two atoms and one bond between them. (C2) force that atoms with smaller indexes exist. (C3) require symmetric A . (C4) only admit bonds between two existing atoms, where $N - 1$ is a big-M constant. (C5) force atom v to be linked with at least one atom with smaller index if atom v exists.

$$A_{0,0} = A_{1,1} = A_{0,1} = 1 \tag{C1}$$

Table 2: Summary of notations used in MIP formulation for CAMD. Their values correspond to the example with four types of atom $\{C, N, O, S\}$.

Symbol	Description	Value
N	number of nodes	*
F	number of features	15
N^t	number of atom types	4
N^n	number of neighbors	4
N^h	number of hydrogen	5
I^t	indexes for N^t	$\{0, 1, 2, 3\}$
I^n	indexes for N^n	$\{4, 5, 6, 7\}$
I^h	indexes for N^h	$\{8, 9, 10, 11, 12\}$
I^{db}	index for double bond	13
I^{tb}	index for triple bond	14
$Atom$	atom types	$\{C, N, O, S\}$
Cov	valences of atom	$\{4, 3, 2, 2\}$

Table 3: List of atom features

$X_{v,f}$	Description
$f \in I^t$	which atom type in $Atom$
$f \in I^n$	number of neighbors, $1 \sim \max\{Cov\}$
$f \in I^h$	number of hydrogen, $0 \sim \max\{Cov\}$
$f = I^{db}$	if v is included with double bond(s)
$f = I^{tb}$	if v is included with triple bond

$$A_{v,v} \geq A_{v+1,v+1}, \quad \forall v \in [N-1] \quad (\text{C2})$$

$$A_{u,v} = A_{v,u}, \quad \forall u, v \in [N], u < v \quad (\text{C3})$$

$$(N-1) \cdot A_{v,v} \geq \sum_{u \neq v} A_{u,v}, \quad \forall v \in [N] \quad (\text{C4})$$

$$A_{v,v} \leq \sum_{u < v} A_{u,v}, \quad \forall v \in [N] \setminus \{0\} \quad (\text{C5})$$

4.3.2. Feasible bond features

Constraints (C6) – (C9) define symmetric double/triple bond matrix with zero diagonal elements. (C10) restrict bond type when this bond exists.

$$DB_{v,v} = 0, \quad \forall v \in [N] \quad (\text{C6})$$

$$DB_{u,v} = DB_{v,u}, \quad \forall u, v \in [N], u < v \quad (\text{C7})$$

$$TB_{v,v} = 0, \quad \forall v \in [N] \quad (\text{C8})$$

$$TB_{u,v} = TB_{v,u}, \quad \forall u, v \in [N], u < v \quad (\text{C9})$$

$$DB_{u,v} + TB_{u,v} \leq A_{u,v}, \quad \forall u, v \in [N], u < v \quad (\text{C10})$$

4.3.3. Feasible atom features

If atom v exists, i.e., $A_{v,v} = 1$, then constraints (C11) – (C13) excludes more than one atom type, fixes the number of neighbors, and sets the number of associated hydrogen atoms.

$$A_{v,v} = \sum_{f \in I^t} X_{v,f}, \quad \forall v \in [N] \quad (\text{C11})$$

$$A_{v,v} = \sum_{f \in I^n} X_{v,f}, \quad \forall v \in [N] \quad (\text{C12})$$

$$A_{v,v} = \sum_{f \in I^h} X_{v,f}, \quad \forall v \in [N] \quad (\text{C13})$$

4.3.4. Compatibility between atoms and bonds

Constraints (C14) match the number of neighbors calculated from the adjacency matrix and atom features. (C15) – (C20) consider the compatibility between atom features and bond features. (C21) are the covalence equations.

$$\sum_{u \neq v} A_{u,v} = \sum_{i \in [N^n]} (i+1) \cdot X_{v,I_i^n}, \quad \forall v \in [N] \quad (\text{C14})$$

$$3 \cdot DB_{u,v} \leq X_{u,I^{db}} + X_{v,I^{db}} + A_{u,v}, \quad \forall u, v \in [N], u < v \quad (\text{C15})$$

$$3 \cdot TB_{u,v} \leq X_{u,I^{tb}} + X_{v,I^{tb}} + A_{u,v}, \quad \forall u, v \in [N], u < v \quad (\text{C16})$$

$$\sum_{u \in [N]} DB_{u,v} \leq \sum_{i \in [N^t]} \left\lfloor \frac{Cov_i}{2} \right\rfloor \cdot X_{v,I_i^t}, \quad \forall v \in [N] \quad (\text{C17})$$

$$\sum_{u \in [N]} TB_{u,v} \leq \sum_{i \in [N^t]} \left\lfloor \frac{Cov_i}{3} \right\rfloor \cdot X_{v,I_i^t}, \quad \forall v \in [N] \quad (\text{C18})$$

$$X_{v,I^{db}} \leq \sum_{u \in [N]} DB_{u,v}, \quad \forall v \in [N] \quad (\text{C19})$$

$$X_{v,I^{tb}} \leq \sum_{u \in [N]} TB_{u,v}, \quad \forall v \in [N] \quad (\text{C20})$$

$$\begin{aligned} \sum_{i \in [N^t]} Cov_i \cdot X_{v,I_i^t} &= \sum_{i \in [N^n]} (i+1) \cdot X_{v,I_i^n} \\ &+ \sum_{i \in [N^h]} i \cdot X_{i,I_i^h} \\ &+ \sum_{u \in [N]} DB_{u,v} + \sum_{u \in [N]} 2 \cdot TB_{u,v}, \quad \forall v \in [N] \end{aligned} \quad (\text{C21})$$

4.3.5. Avoiding spurious extrapolation

Constraints (C22) – (C25) bound the number of each type of atom, double/triple bonds, and rings using observations from the dataset. By setting proper bounds, we can control the composition of the molecule, and avoid extreme cases such as all atoms being set to oxygen, or a molecule with too many rings or double/triple bounds.

$$\sum_{v \in [N]} X_{v,I_i^t} \in [LB_{Atom_i}, UB_{Atom_i}], \quad \forall i \in [N^t] \quad (\text{C22})$$

$$\sum_{v \in [N]} \sum_{u < v} DB_{u,v} \in [LB_{db}, UB_{db}] \quad (\text{C23})$$

$$\sum_{v \in [N]} \sum_{u < v} TB_{u,v} \in [LB_{tb}, UB_{tb}] \quad (\text{C24})$$

$$\sum_{v \in [N]} \sum_{u < v} A_{u,v} - (N-1) \in [LB_{ring}, UB_{ring}] \quad (\text{C25})$$

4.4. Symmetry-breaking constraints

Since the properties of molecules are not influenced by the indexing of molecular graph structure, the score functions and/or models used in CAMD



Figure 2: A molecule (2-methylaziridine or propylene imine) with $N = 4$ heavy atoms corresponds to $N! = 24$ different indexing possibilities.

should be permutational invariant. Training models for CAMD benefits from this invariance since different indexing result in the same performance. However, to consider an optimization problem defined over these models, such as (OPT), each indexing of the same molecule corresponds to a different solution. See Figure 2 as an example. These symmetric solutions significantly enlarge the search space and slow down the solving process.

To handle the symmetry, Zhang et al. (2023) propose symmetry-breaking constraints. As illustrated in Figure 3, the key ideas underlying these constraints are:

- (S1) All subgraphs induced by nodes $\{0, 1, \dots, v\}$ are connected.
- (S2) Node 0 has the most special features compared to other nodes.
- (S3) Node v has neighbors with smaller indexes compared to node $v + 1$.

Among these constraints, (S1) and (S3) are irrelevant to features since they focus on graph indexing. To apply (S2), an application-specific function h needs to be defined to assign a hierarchy to each node based on its features. The case studies give examples of constructing h . Note that these constraints are not limited to CAMD: the constraints apply to any graph-based decision-making problems with symmetry issue caused by graph isomorphism.

Among constraints (C1) - (C25), constraints (C5) are the realization of (S1). Except for (C5), these structural constraints are independent of the graph indexing. Therefore, we can compatibly implement constraints (S2) and (S3) to break symmetry. However, we still need to ensure that there exists at least one feasible indexing for any graph after applying these constraints. Otherwise, the diversity of the feasible set will be reduced, which is unacceptable. We proved that there exists at least one indexing satisfying both (S1) and (S3) for any graph with one node indexed 0 (Zhang et al., 2023). If applying (S2) to choose node 0, then we obtain the desired feasible indexing. Figure 4 shows how to yield a feasible indexing.

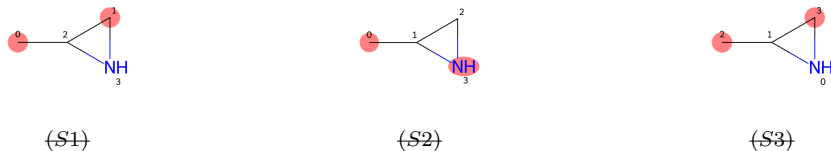


Figure 3: Applying symmetry-breaking constraints to the 2-methylaziridine example. (S1): one of the 10/24 solutions violating (S1), because node 1 is not linked with node 0. (S2): one of the 11/13 solutions violating (S2), because the nitrogen atom is not indexed 0. (S3): one of the 2/3 solutions violating (S3), because $\mathcal{N}(2) = \{1\}$ but $\mathcal{N}(3) = \{0, 1\}$.

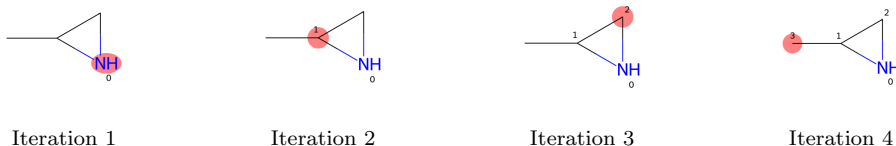


Figure 4: Using the algorithm in Zhang et al. (2023) to index 2-methylaziridine.

Corresponding to (S2), we add the following constraints over features:

$$\sum_{f \in [F]} 2^{F-f-1} \cdot X_{0,f} \leq \sum_{f \in [F]} 2^{F-f-1} \cdot X_{v,f} + 2^F \cdot (1 - A_{v,v}), \quad \forall v \in [N] \setminus \{0\}, \quad (\text{C26})$$

where 2^{F-f-1} , $f \in [F]$ are coefficients to help build a bijective h between all possible features and all integers in $[0, 2^F - 1]$. These coefficients are also called a “universal ordering vector” (Friedman, 2007; Hojny and Pfetsch, 2019). Note that rearranging these coefficients will not influence the bijectivity of h , which will be used in our case studies. The extra term $2^F \cdot (1 - A_{v,v})$ is introduced to exclude non-existent atoms.

On the graph level, constraints (S3) can equivalently be rewritten as:

$$\sum_{u \neq v, v+1} 2^{N-u-1} \cdot A_{u,v} \geq \sum_{u \neq v, v+1} 2^{N-u-1} \cdot A_{u, v+1}, \quad \forall v \in [N-1] \setminus \{0\}. \quad (\text{C27})$$

Similarly, the coefficients 2^{N-u-1} , $u \in [N]$ are used to build a bijective mapping between all possible sets of neighbors and all integers in $[0, 2^N - 1]$.

5. Case studies

The mixed-integer optimization formulation for CAMD introduced in Section 4 only presents the minimal requirements to molecular design. More

specific constraints in real-world problems are not included. Moreover, there are two main limitations in Zhang et al. (2023):

- Problem size: we only solved the optimization problems with up to $N = 8$ atoms, which are too small for most molecular design applications.
- Aromaticity: we only considered double and triple bonds. Aromatic rings are incompatible with (C1) – (C27).

To circumvent these limitations, instead of assembling atoms to form a molecule, we use the concept of molecular fragmentation (Jin et al., 2018, 2020; Podda et al., 2020; Green et al., 2021; Powers et al., 2022). By introducing aromatic rings as different types of fragments, we can design larger molecules with aromaticity. Note that all structural constraints in Section 4.3 and symmetry-breaking constraints in Section 4.4 are still useful. As shown in Table 4, by replacing all atom types and their valences in Table 2 with fragment types and their number of attachment positions, the whole framework is ready for fragment-based molecular design.

This section studies odorant molecules based on the Sharma et al. (2021) dataset. Within that study, odorant molecules and corresponding olfactory annotations collected from different sources were compiled to a single harmonized resource. The dataset contains 4682 molecules, spanning over 104 unique odors, of which two (banana and garlic) were selected for further assessment. Molecules not annotated for a specific odor were assigned the corresponding negative class label. As our formulation focuses on the graph representation without stereo information of molecules, stereo-isomers with contradicting label assignment were removed for the corresponding endpoint. Likewise inorganic compounds or compound mixtures were disregarded in the further analysis. The reasons for testing our approach on both odors are:

1. Showing the compatibility of our CAMD formulation: different odors have different groups of fragments and specific chemical interests.
2. Considering the diversity of the applications: banana is an example of fruity, sweat smell, and garlic represents repelling smells.

The constraints applied so far, i.e., (C1) – (C25), are mainly of syntactical and very generic nature for theoretic organic molecules. However, there are more specific chemical groups and structures that are unfeasible due to various reasons, including chemical instability, reactivity, synthesizability, or are just unsuited for a desired application. Ideally, the trained GNNs

would already capture all those inherent “rules” and subtleties. Obviously, this is never the case in a practical setup. In contrast, most interesting applications are located in low data regimes, so the GNNs will often recognize patterns that are important for the applications but might be poor with regard to chemical plausibility. Thus, in a typical de novo design using a model for scoring, a common approach is to add additional constraints based e.g., on SMARTS (Daylight Chemical Information Systems, Inc., 2007) queries or other simple molecular properties and substructures. This might be done iteratively based on observed structures to additionally add chemical expert knowledge to improve the guidance of de novo design. In the mixed-integer optimization, we can apply additional constraints to narrow down the search space to produce mainly feasible compounds with regard to the desired applications.

5.1. Case 1: Molecules with banana odor

We first fragment all molecules with banana odor in the dataset by cutting all non-aromatic bonds. Since there are only two types of single atoms: C,O, and two types of aromatic rings: *C1CCCO1, *C1CCC(*)C(*)C1, we skip the fragment selection step. The first row of Table 5 describes $F = 14$ features for each fragment.

To design more reasonable molecules with banana odor, we introduce some chemical requirements to shrink the search space.

Requirement 5.1.1 The designed molecule should have at least one of: an aromatic fragment or an oxygen atom linked with double bond. This is based on a visual inspection of molecules with banana odor, where the majority features one of those groups. Mathematically, it requires:

$$\exists v \in [N], \text{ s.t. } X_{v,2} + X_{v,3} \geq 1 \text{ or } X_{v,1} + X_{v,13} \geq 2.$$

To formulate this constraint, we begin by considering the symmetry-breaking constraints (C26) on feature level:

$$\sum_{f \in [F]} h_f \cdot X_{0,f} \leq \sum_{f \in [F]} h_f \cdot X_{v,f} + 2^F \cdot (1 - A_{v,v}), \quad \forall v \in [N] \setminus \{0\}, \quad (\text{B1})$$

where coefficients $h_f, f \in [F]$ are the rearrangement of $2^{F-f-1}, f \in [F]$ as shown in the third row of Table 5. The purpose for assigning these coefficients in this specific way is to make sure that if there is either one aromatic fragment or an oxygen atom linked with double bond, its index must be 0. If

Table 4: Summary of notations used in MIP formulation for fragment-based molecular design. Use the banana odor as an example to provide values for these parameters.

Symbol	Description	Value
N	number of fragments	*
F	number of features	14
N^t	number of fragment types	4
N^n	number of neighbors	4
N^h	number of hydrogen	5
I^t	indexes for N^t	{0, 1, 2, 3}
I^n	indexes for N^n	{4, 5, 6, 7}
I^h	indexes for N^h	{8, 9, 10, 11, 12}
I^{db}	index for double bond	13
$Frag$	fragment types	fragment set
Cov	number of attachment positions	{4, 2, 1, 3}
fragment set: {C,O,*C1CCCO1, *C1CCC(*)C(*)C1}		

Table 5: Description of fragment features and corresponding coefficients for banana odor. The fragment types are {C,O,*C1CCCO1, *C1CCC(*)C(*)C1}. The *=* column denotes that if fragment v is linked with any double bond. Triple bonds are not considered since no molecule with banana odor in the dataset contains triple bond(s).

$X_{v,f}$	fragment type				# neighbors				#hydrogen					*=*
f	0	1	2	3	4	5	6	7	8	9	10	11	12	13
h_f	2^{13}	2^{12}	2^{11}	2^{10}	2^6	2^7	2^8	2^9	2^1	2^2	2^3	2^4	2^5	2^0

fragment 0 is an oxygen atom, to make sure it is linked with a double bond (which means that it has one neighbor and no hydrogen atom), we can add the following constraint:

$$\sum_{f \in [F]} h_f \cdot X_{0,f} \leq \underbrace{2^{12}}_{\text{oxygen}} + \underbrace{2^6}_{1 \text{ neighbor}} + \underbrace{2^1}_{0 \text{ hydrogen}} + \underbrace{2^0}_{\text{double bond}}, \quad (\text{B2})$$

which also includes the cases with at least one aromatic ring.

5.2. Case 2: Molecules with garlic odor

For molecules with garlic odor, there are four types of atoms: C, N, S, O, and three types of fragments: *C1CCCCC1*, *C1CCC(*)O1, *C1CCSC1. Therefore, there are $F = 17$ features for each fragment, i.e., 7 for fragment type, 4 for number of neighbors, 5 for number of hydrogen atoms, and 1 for double bond.

For garlic odor, we propose the following requirements and corresponding constraints.

Requirement 5.2.1 Any atom in {C, N, S, O} can not be associated with two or more atoms in {N, S, O} with single bonds. This requirement is included as the optimization results showed a tendency to include a huge amount of connected heteroatoms in suggested structures. While we might also exclude some chemically feasible molecules with this generic restriction, such structures are often either unstable or reactive. Equivalently, we have:

$$\underbrace{\sum_{f=1}^3 X_{u,f}}_{u \in \{N,S,O\}} + \underbrace{\sum_{f=0}^3 X_{v,f}}_{v \in \{C,N,S,O\}} + \underbrace{\sum_{f=1}^3 X_{w,f}}_{w \in \{N,S,O\}} + \underbrace{(A_{u,v} - DB_{u,v})}_{u-v} + \underbrace{(A_{v,w} - DB_{v,w})}_{v-w} \leq 4, \quad \forall u \neq v \neq w \in [N]. \quad (\text{G1})$$

Requirement 5.2.2 Sulfur atom is only linked with carbon atom(s). The reason for introducing this requirement is similar as for Requirement 1, to reduce accumulations of heteroatoms by excluding heteroatom-heteroatom single bonds in the search space. That is, atom S can not be linked with atom(s) in {N, S, O}. Similar to (G2), we add constraints defined by:

$$\underbrace{X_{v,2}}_{v=S} + \underbrace{\sum_{f=1}^3 X_{u,f}}_{u \in \{N,S,O\}} + \underbrace{A_{u,v}}_{u-v} \leq 2, \quad \forall u \neq v \in [N]. \quad (\text{G2})$$

5.3. Extra constraints

After applying constraints introduced in Section 5.1 and Section 5.2, we still find several impractical molecular structures. This section introduces extra constraints for both odors based on different considerations.

Requirement 5.3.1 No double bond is linked with an aromatic ring. Since constraints (C17) already limit the maximal number of double bonds for each fragment, we only need to consider fragments with more than 1 attachment positions. For banana odor, we exclude cases where fragment *C1CCC(*)C(*)C1 is linked with a double bond, i.e.,

$$X_{v,3} + X_{v,13} \leq 1, \forall v \in [N]. \quad (\text{B3})$$

For garlic odor, *C1CCCCC1* and *C1CCC(*)O1 should be considered, i.e.,

$$X_{v,4} + X_{v,5} + X_{v,16} \leq 1, \forall v \in [N]. \quad (\text{G3})$$

Requirement 5.3.2 Exclude allenes due to their instability, i.e., a carbon atom associated with two double bonds. This requirement can be implemented by restricting constraints (C19) into equations:

$$X_{v,db} = \sum_{u \in [N]} DB_{u,v}, \forall v \in [N]. \quad (\text{C19}')$$

Requirement 5.3.3 Oxygen atom is not allowed to link with another oxygen atom. We introduce (B4) to banana odor and (G4) to garlic odor due to different feature index of oxygen atom, where (B4) is defined as:

$$\underbrace{X_{v,1}}_{v=O} + \underbrace{X_{u,1}}_{u=O} + \underbrace{A_{u,v}}_{u-v} \leq 2, \forall u \neq v \in [N]. \quad (\text{B4})$$

and (G4) is defined as:

$$\underbrace{X_{v,3}}_{v=O} + \underbrace{X_{u,3}}_{u=O} + \underbrace{A_{u,v}}_{u-v} \leq 2, \forall u \neq v \in [N]. \quad (\text{G4})$$

Requirement 5.3.4 We set the maximum number of aromatic rings as 2 to avoid big molecules, which have low vapor pressure and thus would hardly form gasses which can be smelled. For banana odor, this bound is:

$$\sum_{v \in [N]} (X_{v,2} + X_{v,3}) \leq 2. \quad (\text{B5})$$

For garlic odor, this bound is:

$$\sum_{v \in [N]} (X_{v,4} + X_{v,5} + X_{v,6}) \leq 2. \quad (\text{G5})$$

6. Numerical results

GNNs are implemented and trained in PyG (Fey and Lenssen, 2019). Mixed-integer formulation of CAMD is implemented based on our extension to OMLT described in Section 3. All optimization problems are solved using Gurobi 10.0.1 (Gurobi Optimization, LLC, 2023). All experiments are conducted in the Imperial College London High Performance Computing server. Each optimization problem is solved with a node with AMD EPYC 7742 (64 cores and 64GB memory).

6.1. Data preparation and model training

As shown in Section 5, for each target odor (from banana and garlic) in the dataset from Sharma et al. (2021), we first fragment all molecules with target odor, then construct features for each fragment and build graph representation on fragment level. After these steps, we have data in the positive class, i.e., with target odor.

To select data in the negative class, we fragment all molecules without the target odor, and choose molecules consisting of the same set of fragments as the negative class. Since there are many more molecules in the negative class than the positive class, we set the following constraints to filter these molecules:

- The upper bound for the number of each type of atom except for C, e.g., N, S, O, is half the number of fragments, i.e., $N/2$.
- The upper bound for the number of aromatic rings is 2.
- The upper bound for the number of double bonds is $N/2$.
- With banana as the target odor, each molecule should have either one aromatic ring or an oxygen atom linked with double bond.
- With garlic as the target odor, each molecule should have either one aromatic ring or a sulfur atom.

There are 1278 molecules consisting of the same group of fragments but without banana odor, 190 out of which are chosen as the negative class after applying those constraints. Combining with 110 molecules with banana odor, we have 300 molecules for the study of banana odor. For garlic odor, 179

among 1449 molecules are chosen as the negative class. Together with 83 molecules in the positive class, we have 262 molecules for garlic odor.

For each odor, we train a GNN that consists of two SAGEConv layers with 16 hidden features, a mean pooling, and a dense layer as a final classifier. For statistical consideration, we train 10 models with different random seeds for each odor. The average training/testing accuracy is 0.905/0.703 for banana odor, and 0.997/0.846 for garlic odor.

6.2. Optimality: Find optimal molecules

Our optimization goal is to design molecules with the target odor. Denote y_0 and y_1 as the logits of those trained GNNs. Then the objective function is $y_1 - y_0$. Maximizing this objective is equivalent to maximizing the probability of assigning an input molecule to positive class. Together with constraints listed in Section 4 and Section 5, our optimization problem is:

$$\begin{aligned} & \max_{(X,A)} y_1 - y_0 \\ & \text{s.t. } (y_0, y_1) = GNN(X, A), \\ & \quad \text{(C1) - (C25), (C19')}, \\ & \quad \text{(C27), (B1) - (B5) (banana),} \\ & \quad \text{(C26), (C27), (G1) - (G5) (garlic).} \end{aligned}$$

For each model with a given N , we solve the corresponding optimization problem 5 times with different random seeds in Gurobi. Each run uses the default relative MIP optimality gap, i.e., 10^{-4} , and a 10 hour time limit. Figure 5 shows the time cost for designing molecules with up to 12 fragments. Figures 6 and 7 plot the molecules corresponding to the best solutions found within the time limit. Tables 6 and 7 report full experimental details.

6.3. Feasibility: Towards larger design

As shown in Tables 6 and 7, the increasing dimension and complexity of the optimization problems make solving to optimality intractable with larger N . Practically, however, the optimality is not the only priority. A feasible solution with good prediction is also acceptable. In this section, instead of considering optimality, we restrict the time limit to 5 hours and report the best solutions found within the time limit for larger N , i.e., $15 \leq N \leq 50$. By setting MIPFocus=1 in Gurobi, we tend to find feasible solutions

Table 6: Numerical results for banana odor. For each N , numbers of variables ($\#var_c$: continuous, $\#var_b$: binary) and constraints ($\#con$) after presolve stage in Gurobi are first reported. Then we count the number of successful runs ($\#run$) over 50 runs, i.e., achieving relative MIP optimality gap 10^{-4} . For all successful runs, we provide the 25th percentile (Q_1), mean, and 75th percentile (Q_3) of the running time $time_{tol}$ as well as the first time to find the optimal solution $time_{opt}$. The time limit for each run is 10 hours. Except for the time limit and random seed, we use the default setting in Gurobi for other parameters such as the tolerance.

N	$\#var_c$	$\#var_b$	$\#con$	$\#run$	$time_{opt}$ (s)			$time_{tol}$ (s)		
					mean	Q_1	Q_3	mean	Q_1	Q_3
4	478	170	1231	50	3	0	4	5	4	5
5	733	224	1939	50	7	6	9	9	8	10
6	1172	280	2931	50	18	13	18	23	15	20
7	1573	336	3972	50	96	52	121	121	76	146
8	1969	391	5063	50	292	171	374	426	306	546
9	2410	448	6287	50	886	380	1343	1473	792	1679
10	2909	507	7687	50	4204	1990	5291	6237	3736	7104
11	3466	568	9263	41	10686	3684	16495	15954	6815	25038
12	4023	629	10839	9	14869	6461	21331	21415	13923	25480

Table 7: Numerical results for garlic odor.

N	$\#var_c$	$\#var_b$	$\#con$	$\#run$	$time_{opt}$ (s)			$time_{tol}$ (s)		
					mean	Q_1	Q_3	mean	Q_1	Q_3
4	516	187	1363	50	5	4	6	6	5	7
5	811	248	2251	50	12	9	14	21	12	23
6	1315	306	3403	50	65	17	93	108	41	137
7	1759	365	4609	50	214	105	241	383	221	484
8	2204	424	5916	50	1301	198	1247	2397	776	3191
9	2694	484	7345	44	7318	1278	9712	10387	2940	14203
10	3237	546	8962	20	11188	2862	17619	13948	5561	18792
11	3844	609	10790	8	9521	3686	17850	12539	4971	21075
12	4515	674	12833	5	20774	17136	23344	32475	31034	34172

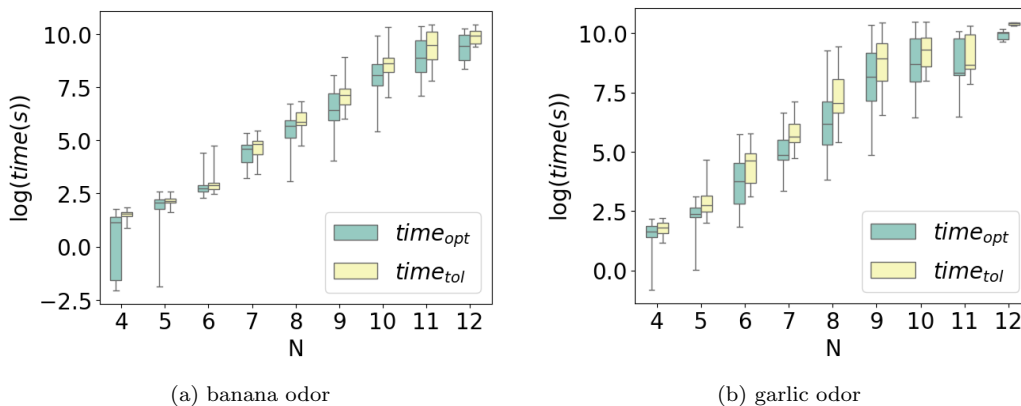


Figure 5: These graphs report time_{opt} and time_{tol} averaged over the number of successful runs among 50 runs for both odors. time_{opt} is the first time to find the optimal solution, time_{tol} is the total running time.

quickly instead of proving optimality. Also, for each model, we only solve the corresponding optimization problem once due to its large size.

As shown in Figure 8, when $N \leq 25$, a positive objective value, i.e., a molecule with target odor, can be found for most runs. When $30 \leq N \leq 40$, however, the solutions are mostly negative, which are unlikely desired odorant molecules. The possible reason is that finding a feasible solution is already hard with such large problem, and there is not enough time for the solver to find better solutions. With even large problems for $N > 40$, feasibility becomes impractical: only 1 run finds a feasible solution among 20 runs for both odors. For instance, when $N = 50$ for garlic odor, there are 9.57×10^4 variables (8.82×10^4 continuous, 7.45×10^3 binary) and 4.67×10^5 constraints.

7. Conclusions

This paper considers optimization-based molecular design with GNNs using MIP. To include GNNs into our optimization problems, we propose big-M formulation for GNNs and implement the encodings into open-resource software tool OMLT. To reduce the design space, we introduce symmetry-breaking constraints to remove symmetric solutions caused by graph isomorphism, i.e., one molecule has many different indexing. For case studies, we consider fragment-based design to include aromaticity and discover larger molecules. Specific chemical requirements are considered and mathematically represented as linear constraints for both cases. Numerical results show

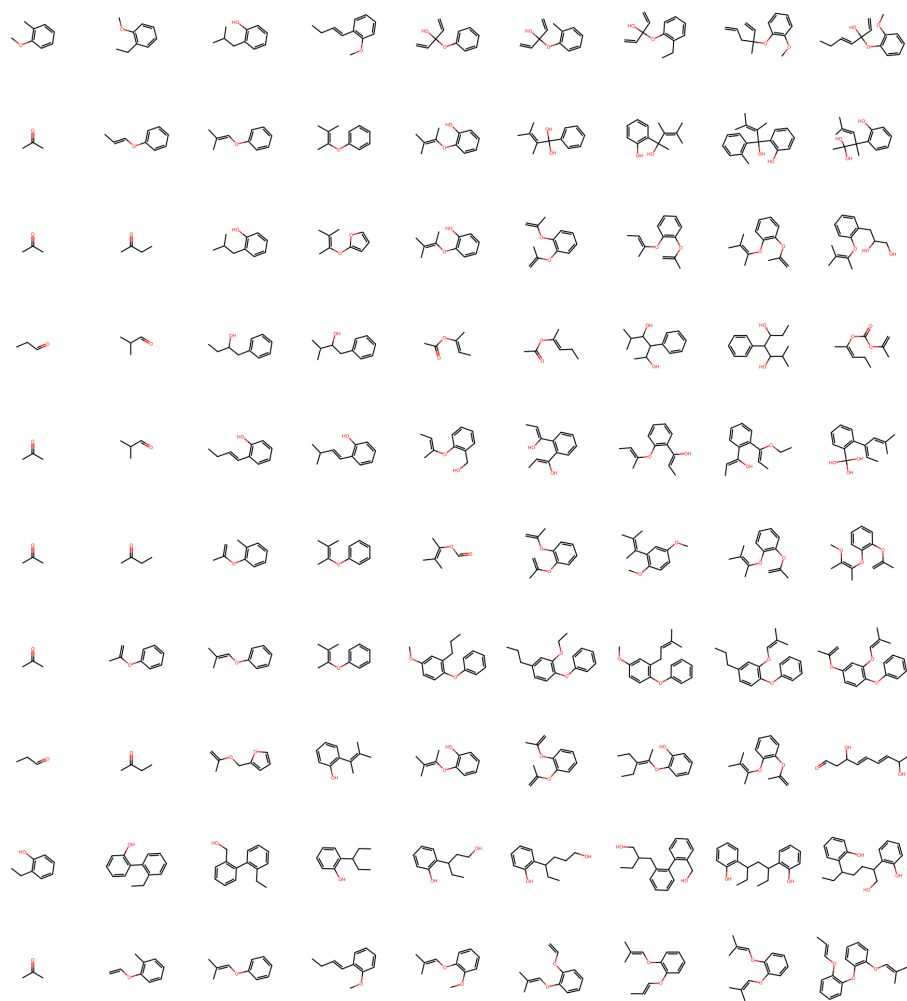


Figure 6: Results for banana odor. Each molecule is the best solution found after 10 hours for a model with a given N . Each row corresponds to the same model, and each column corresponds to the same N ranging from 4 to 12.



Figure 7: Results for garlic odor. Each molecule is the best solution found after 10 hours for a model with a given N . Each row corresponds to the same model, and each column corresponds to the same N ranging from 4 to 12.

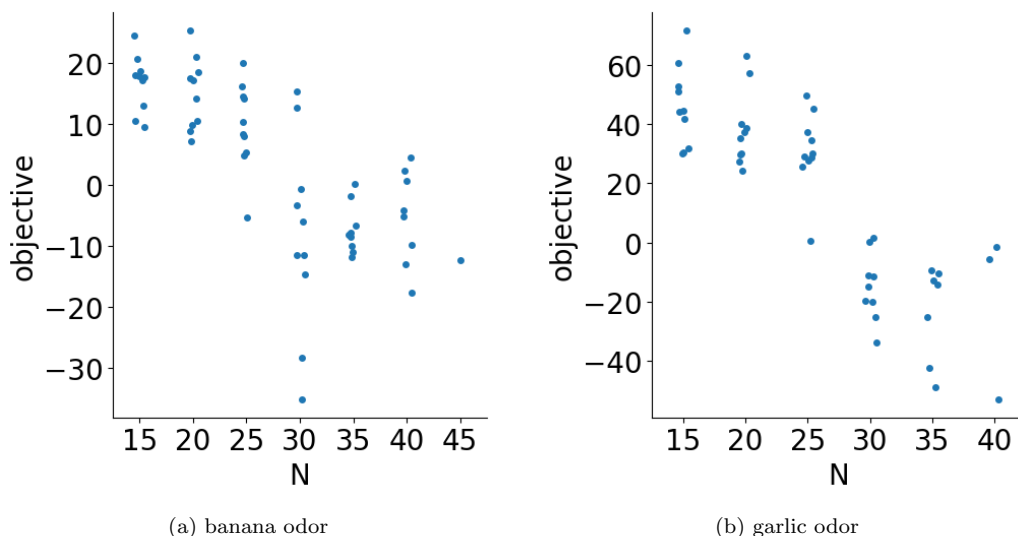


Figure 8: These graphs report the best objective values found within 5 hours for 10 models with $15 \leq N \leq 50$. Each point corresponds to the molecule found from one model.

that we can find the optimal molecules with up to 12 fragments. Without pursuing optimality, our approach can find larger molecules with good predictions.

8. Acknowledgements

This work was supported by the Engineering and Physical Sciences Research Council [grant numbers EP/W003317/1], an Imperial College Hans Rausing PhD Scholarship to SZ, and a BASF/RAEng Research Chair in Data-Driven Optimisation to RM.

References

- Albawi, S., Mohammed, T.A., Al-Zawi, S., 2017. Understanding of a convolutional neural network, in: ICET.
- Alshehri, A.S., Gani, R., You, F., 2020. Deep learning and knowledge-based methods for computer-aided molecular design — toward a unified approach: State-of-the-art and future directions. *Computers & Chemical Engineering* 141, 107005.

- Alshehri, A.S., Tula, A.K., Zhang, L., Gani, R., You, F., 2021. A platform of machine learning-based next-generation property estimation methods for CAMD, in: *Computer Aided Chemical Engineering*. volume 50, pp. 227–233.
- Ammari, B.L., Johnson, E.S., Stinchfield, G., Kim, T., Bynum, M., Hart, W.E., Pulsipher, J., Laird, C.D., 2023. Linear model decision trees as surrogates in optimization of engineering applications. *Computers & Chemical Engineering* 178.
- Anderson, R., Huchette, J., Ma, W., Tjandraatmadja, C., Vielma, J.P., 2020. Strong mixed-integer programming formulations for trained neural networks. *Mathematical Programming* 183, 3–39.
- Atwood, J., Towsley, D., 2016. Diffusion-convolutional neural networks, in: *NeurIPS*.
- Austin, N.D., Sahinidis, N.V., Trahan, D.W., 2016. Computer-aided molecular design: An introduction and review of tools, applications, and solution techniques. *Chemical Engineering Research and Design* 116, 2–26.
- Botoeva, E., Kouvaros, P., Kronqvist, J., Lomuscio, A., Misener, R., 2020. Efficient verification of ReLU-based neural networks via dependency analysis, in: *AAAI*.
- Bruna, J., Zaremba, W., Szlam, A., Lecun, Y., 2014. Spectral networks and locally connected networks on graphs, in: *ICLR*.
- Bunel, R., Mudigonda, P., Turkaslan, I., Torr, P., Lu, J., Kohli, P., 2020a. Branch and bound for piecewise linear neural network verification. *Journal of Machine Learning Research* 21.
- Bunel, R.R., Hinder, O., Bhojanapalli, S., Dvijotham, K., 2020b. An efficient nonconvex reformulation of stagewise convex optimization problems. *NeurIPS* .
- Bunel, R.R., Turkaslan, I., Torr, P., Kohli, P., Mudigonda, P.K., 2018. A unified view of piecewise linear neural network verification. *NeurIPS* .
- Bynum, M.L., Hackebeitl, G.A., Hart, W.E., Laird, C.D., Nicholson, B.L., Sirola, J.D., Watson, J.P., Woodruff, D.L., et al., 2021. *Pyomo - Optimization Modeling in Python*. volume 67. Springer.

- Camarda, K.V., Maranas, C.D., 1999. Optimization in polymer design using connectivity indices. *Industrial & Engineering Chemistry Research* 38, 1884–1892.
- Ceccon, F., Jalving, J., Haddad, J., Thebelt, A., Tsay, C., Laird, C.D., Misener, R., 2022. OMLT: Optimization & machine learning toolkit. *Journal of Machine Learning Research* 23, 15829–15836.
- Cheun, J.Y., Liew, J.Y.L., Tan, Q.Y., Chong, J.W., Ooi, J., Chemmangattuvalappil, N.G., 2023. Design of polymeric membranes for air separation by combining machine learning tools with computer aided molecular design. *Processes* 11, 2004.
- Chong, J.W., Thangalazhy-Gopakumar, S., Muthoosamy, K., Chemmangattuvalappil, N.G., 2022. Design of bio-oil solvents using multi-stage computer-aided molecular design tools, in: *Computer Aided Chemical Engineering*. volume 49, pp. 199–204.
- Churi, N., Achenie, L.E., 1996. Novel mathematical programming model for computer aided molecular design. *Industrial & Engineering Chemistry Research* 35, 3788–3794.
- Daylight Chemical Information Systems, Inc., 2007. SMARTS - A language for describing molecular patterns.
- Defferrard, M., Bresson, X., Vandergheynst, P., 2016. Convolutional neural networks on graphs with fast localized spectral filtering, in: *NeurIPS*.
- Delarue, A., Anderson, R., Tjandraatmadja, C., 2020. Reinforcement learning with combinatorial actions: An application to vehicle routing, in: *NeurIPS*.
- Duvenaud, D.K., Maclaurin, D., Iparraguirre, J., Bombarell, R., Hirzel, T., Aspuru-Guzik, A., Adams, R.P., 2015. Convolutional networks on graphs for learning molecular fingerprints, in: *NeurIPS*.
- Elton, D.C., Boukouvalas, Z., Fuge, M.D., Chung, P.W., 2019. Deep learning for molecular design — a review of the state of the art. *Molecular Systems Design & Engineering* 4, 828–849.

- Faez, F., Ommi, Y., Baghshah, M.S., Rabiee, H.R., 2021. Deep graph generators: A survey. *IEEE Access* 9, 106675–106702.
- Fey, M., Lenssen, J.E., 2019. Fast graph representation learning with PyTorch Geometric, in: *ICLR 2019 Workshop on Representation Learning on Graphs and Manifolds*.
- Fischetti, M., Jo, J., 2018. Deep neural networks and mixed integer linear optimization. *Constraints* 23, 296–309.
- Friedman, E.J., 2007. Fundamental domains for integer programs with symmetries, in: *Combinatorial Optimization and Applications*.
- Gani, R., 2004. Computer-aided methods and tools for chemical product design. *Chemical Engineering Research and Design* 82, 1494–1504.
- Gani, R., Zhang, L., Gounaris, C., 2022. Editorial overview: Frontiers of chemical engineering: chemical product design II. *Current Opinion in Chemical Engineering* 35, 100783.
- Gao, W., Fu, T., Sun, J., Coley, C.W., 2022. Sample efficiency matters: A benchmark for practical molecular optimization, in: *NeurIPS Track Datasets and Benchmarks*.
- Gilmer, J., Schoenholz, S.S., Riley, P.F., Vinyals, O., Dahl, G.E., 2017. Neural message passing for quantum chemistry, in: *ICML*.
- Green, H., Koes, D.R., Durrant, J.D., 2021. DeepFrag: a deep convolutional neural network for fragment-based lead optimization. *Chemical Science* 12, 8036–8047.
- Gurobi Optimization, LLC, 2023. Gurobi Optimizer Reference Manual. URL: <https://www.gurobi.com>.
- Hamilton, W., Ying, Z., Leskovec, J., 2017. Inductive representation learning on large graphs, in: *NeurIPS*.
- Hatamleh, M., Chong, J.W., Tan, R.R., Aviso, K.B., Janairo, J.I.B., Chemmangattuvalappil, N.G., 2022. Design of mosquito repellent molecules via the integration of hyperbox machine learning and computer aided molecular design. *Digital Chemical Engineering* 3, 100018.

- Hojny, C., Pfetsch, M.E., 2019. Polytopes associated with symmetry handling. *Mathematical Programming* 175, 197–240.
- Horvath, B., Muguruza, A., Tomas, M., 2021. Deep learning volatility: A deep neural network perspective on pricing and calibration in (rough) volatility models. *Quantitative Finance* 21, 11–27.
- Huchette, J., Muñoz, G., Serra, T., Tsay, C., 2023. When deep learning meets polyhedral theory: A survey. *arXiv preprint arXiv:2305.00241* .
- Jin, W., Barzilay, R., Jaakkola, T., 2018. Junction tree variational autoencoder for molecular graph generation, in: *ICML*.
- Jin, W., Barzilay, R., Jaakkola, T., 2020. Hierarchical generation of molecular graphs using structural motifs, in: *ICML*.
- Kipf, T.N., Welling, M., 2017. Semi-supervised classification with graph convolutional networks, in: *ICLR*.
- Liu, Q., Zhang, L., Liu, L., Du, J., Tula, A.K., Eden, M., Gani, R., 2019. OptCAMD: An optimization-based framework and tool for molecular and mixture product design. *Computers & Chemical Engineering* 124, 285–301.
- Mann, V., Gani, R., Venkatasubramanian, V., 2023. Group contribution-based property modeling for chemical product design: A perspective in the AI era. *Fluid Phase Equilibria* 568, 113734.
- McDonald, T., Tsay, C., Schweidtmann, A.M., Yorke-Smith, N., 2023. Mixed-integer optimisation of graph neural networks for computer-aided molecular design. *arXiv preprint arXiv:2312.01228* .
- Mišić, V.V., 2020. Optimization of tree ensembles. *Operations Research* 68, 1605–1624.
- Mistry, M., Letsios, D., Krennrich, G., Lee, R.M., Misener, R., 2021. Mixed-integer convex nonlinear optimization with gradient-boosted trees embedded. *INFORMS Journal on Computing* 33, 1103–1119.
- Ng, L.Y., Chong, F.K., Chemmangattuvalappil, N.G., 2014. Challenges and opportunities in computer aided molecular design. *Computer Aided Chemical Engineering* 34, 25–34.

- Niepert, M., Ahmed, M., Kutzkov, K., 2016. Learning convolutional neural networks for graphs, in: ICML.
- Odele, O., Macchietto, S., 1993. Computer aided molecular design: A novel method for optimal solvent selection. *Fluid Phase Equilibria* 82, 47–54.
- Papalexopoulos, T.P., Tjandraatmadja, C., Anderson, R., Vielma, J.P., Belanger, D., 2022. Constrained discrete black-box optimization using mixed-integer programming, in: ICML.
- Podda, M., Bacciu, D., Micheli, A., 2020. A deep generative model for fragment-based molecule generation, in: AISTATS.
- Powers, A.S., Yu, H.H., Suriana, P.A., Dror, R.O., 2022. Fragment-based ligand generation guided by geometric deep learning on protein-ligand structures, in: ICLR 2022 Workshop MLDD.
- Rittig, J.G., Ritzert, M., Schweidtmann, A.M., Winkler, S., Weber, J.M., Morsch, P., Heufer, K.A., Grohe, M., Mitsos, A., Dahmen, M., 2022. Graph machine learning for design of high-octane fuels. *AICHe Journal* , e17971.
- Ryu, M., Chow, Y., Anderson, R., Tjandraatmadja, C., Boutilier, C., 2020. CAQL: Continuous action Q-learning, in: ICLR.
- Sahinidis, N.V., Tawarmalani, M., Yu, M., 2003. Design of alternative refrigerants via global optimization. *AICHe Journal* 49, 1761–1775.
- Say, B., Wu, G., Zhou, Y.Q., Sanner, S., 2017. Nonlinear hybrid planning with deep net learned transition models and mixed-integer linear programming, in: IJCAI.
- Schweidtmann, A.M., Rittig, J.G., König, A., Grohe, M., Mitsos, A., Dahmen, M., 2020. Graph neural networks for prediction of fuel ignition quality. *Energy & Fuels* 34, 11395–11407.
- Serra, T., Yu, X., Kumar, A., Ramalingam, S., 2021. Scaling up exact neural network compression by ReLU stability, in: NeurIPS.
- Sharma, A., Kumar, R., Ranjta, S., Varadwaj, P.K., 2021. SMILES to smell: decoding the structure–odor relationship of chemical compounds using the deep neural network approach. *Journal of Chemical Information and Modeling* 61, 676–688.

- Shindo, H., Matsumoto, Y., 2019. Gated graph recursive neural networks for molecular property prediction. arXiv preprint arXiv:1909.00259 .
- Sinha, M., Achenie, L.E., Ostrovsky, G.M., 1999. Environmentally benign solvent design by global optimization. *Computers & Chemical Engineering* 23, 1381–1394.
- Szegedy, C., Zaremba, W., Sutskever, I., Bruna, J., Erhan, D., Goodfellow, I., Fergus, R., 2014. Intriguing properties of neural networks, in: ICLR.
- Thebelt, A., Kronqvist, J., Mistry, M., Lee, R.M., Sudermann-Merx, N., Misener, R., 2021. Entmoot: A framework for optimization over ensemble tree models. *Computers & Chemical Engineering* 151, 107343.
- Tiew, S.T., Chew, Y.E., Lee, H.Y., Chong, J.W., Tan, R.R., Aviso, K.B., Chemmangattuvalappil, N.G., 2023. A fragrance prediction model for molecules using rough set-based machine learning. *Chemie Ingenieur Technik* 95, 438–446.
- Tjeng, V., Xiao, K.Y., Tedrake, R., 2019. Evaluating robustness of neural networks with mixed integer programming, in: ICLR.
- Tsay, C., Kronqvist, J., Thebelt, A., Misener, R., 2021. Partition-based formulations for mixed-integer optimization of trained ReLU neural networks, in: NeurIPS.
- Wang, K., Lozano, L., Cardonha, C., Bergman, D., 2023. Optimizing over an ensemble of trained neural networks. *INFORMS Journal on Computing* .
- Wang, X., Li, Z., Jiang, M., Wang, S., Zhang, S., Wei, Z., 2019. Molecule property prediction based on spatial graph embedding. *Journal of Chemical Information and Modeling* 59, 3817–3828.
- Withnall, M., Lindelöf, E., Engkvist, O., Chen, H., 2020. Building attention and edge message passing neural networks for bioactivity and physical–chemical property prediction. *Journal of Cheminformatics* 12, 1–18.
- Wu, G., Say, B., Sanner, S., 2020. Scalable planning with deep neural network learned transition models. *Journal of Artificial Intelligence Research* 68, 571–606.

- Xia, X., Hu, J., Wang, Y., Zhang, L., Liu, Z., 2019. Graph-based generative models for *de Novo* drug design. *Drug Discovery Today: Technologies* 32, 45–53.
- Xiong, J., Xiong, Z., Chen, K., Jiang, H., Zheng, M., 2021. Graph neural networks for automated *de novo* drug design. *Drug Discovery Today* 26, 1382–1393.
- Xu, Y., Pei, J., Lai, L., 2017. Deep learning based regression and multiclass models for acute oral toxicity prediction with automatic chemical feature extraction. *Journal of Chemical Information and Modeling* 57, 2672–2685.
- Yang, K., Swanson, K., Jin, W., Coley, C., Eiden, P., Gao, H., Guzman-Perez, A., Hopper, T., Kelley, B., Mathea, M., et al., 2019. Analyzing learned molecular representations for property prediction. *Journal of Chemical Information and Modeling* 59, 3370–3388.
- Zhang, L., Cignitti, S., Gani, R., 2015. Generic mathematical programming formulation and solution for computer-aided molecular design. *Computers & Chemical Engineering* 78, 79–84.
- Zhang, S., Campos, J.S., Feldmann, C., Walz, D., Sandfort, F., Mathea, M., Tsay, C., Misener, R., 2023. Optimizing over trained GNNs via symmetry breaking, in: *NeurIPS*.